JOURNAL OF GUIDANCE, CONTROL, AND DYNAMICS
Vol. 33, No. 3, May–June 2010

Target Maneuver Adaptive Guidance Law for a Bounded Acceleration Missile

Ronen Atir,* Gyorgy Hexner,† and Haim Weiss‡
Rafael Advanced Defense Systems, Ltd., 31021 Haifa, Israel
and
Tal Shima§
Technion—Israel Institute of Technology, 32000 Haifa, Israel

DOI: 10.2514/1.47276

A new multiple-model adaptive estimator-guidance law is presented for a bounded acceleration interceptor pursuing a target performing a sudden step maneuver. The estimators proposed for each model in the filter bank differ in the expected timing of the target maneuver jump and feature a mechanism constructed to efficiently identify such a jump. The certainty equivalence principle seems to be invalid in the case of bounded missile acceleration. Hence, the resulting guidance gain for each target model, calculated using an equivalent random input describing function, depends on the measurement noise level, target maneuver statistics, and saturation limit. These gains can be computed a priori and stored in a lookup table to be used online, and are different for each target model in the bank. In contrast, the expressions for the zero-effort miss for all models are identical; however, their *value* is independently evaluated by each estimator in the bank and, hence, are in general different. Simulation results show significant improvement over the deterministic optimal guidance law when jump times vary from 10 to 3 missile time constants before intercept. A sensitivity analysis to various noise levels and expected target maneuvers was carried out, emphasizing the robustness and advantages of this scheme.

I. Introduction

THE most popular and widely used guidance law, proportional navigation (PN), was first introduced by Yuan [1]. PN issues a guidance acceleration command that is jointly proportional to the inertial angular rate of the line of sight (LOS) between the missile and the target, and the missile-to-target closing velocity [2]. Basically, if ideal dynamics are assumed, and there are no acceleration constraints, PN results in zero miss distance. For a nonmaneuvering target, constant missile and target speeds, and ideal dynamics, both the target and the missile move close to straight lines that meet each other at the intercept point. These lines, together with the missile–target LOS, are referred to as the collision triangle. This collision triangle is the basis for a linearized version of the general guidance problem. When both the pursuer and evader follow the collision triangle with small deviations, a linear approximation of the dynamic conflict describes the full conflict kinematics with a reasonable accuracy. This trajectory linearization is usually adequate when dealing with terminal missile guidance, that is, the last few seconds of the intercept.

Although PN is easy to implement, widely used, and might suffice for many applications, it has its drawbacks. For example, in realistic interception scenarios between a pursuer with limited maneuverability and a target with a large maneuver capability, a significant miss distance may result. To achieve a smaller miss distance and to relax the large acceleration requirements, modern guidance laws are formulated. The performance improvements are not free of cost and naturally require additional information to bring forth such an improvement. The additional information includes the predicted time to intercept, or time to go (t_{go}), and missile and target accelerations.

An important concept that arose in the study of modern guidance laws is the zero-effort miss (ZEM). In a one-sided optimal control formulation, the ZEM is the miss distance that would result if the missile made no further corrective commands and the target followed the assumed acceleration model.

The PN guidance law may be expressed using the ZEM concept. The ZEM is constructed assuming the target's acceleration is zero and ideal missile dynamics. The augmented proportional navigation (APN) [2] guidance law suggests an augmentation term (and, hence, its name) compensating for a constant target acceleration by including its effect in the ZEM term. The direct effect of APN, compared to PN, is to reduce the required missile acceleration at the end of the conflict at the expense of a larger acceleration near the initial time. Another benefit of APN is the reduction of the total required maneuver that is equivalent to the control effort.

For a maneuvering target, using optimal control theory, it was proven that, for an ideal dynamics missile, APN with navigation coefficient $N' = 3$ is, in fact, an optimal guidance law. This guidance law minimizes a quadratic cost function of the integral of the square of the missile acceleration, subject to a zero-miss-distance constraint. Actually, it was also shown that for a nonmaneuvering target the optimal guidance law subjected to the same constraints and cost function is PN with the same navigation gain. Removing the ideal missile dynamics assumption, replacing it with first-order dynamics, and exercising the same optimal control tools resulted in the birth of the optimal guidance law (OGL) [3]. The resulting guidance has the same form: a time varying gain, N', times the ZEM. But now the ZEM contains additional terms in both the missile's and the target's acceleration. It takes the pursuer's guidance system dynamics into account and dynamically cancels out its effects [2].

In real-world problems, sensor and system noise are major influences on miss distance in a pursuer–evader scenario. Also, in a realistic scenario, it is reasonable to assume that the pursuer's state is available but with a small error, for use in the guidance law. In contrast, the evader's state is generally not known to the pursuer. Moreover, a well-designed evader guidance law would make the evading target as difficult to predict as possible. Therefore, target

Presented as Paper 6089 at the AIAA Guidance, Navigation, and Control Conference, Chicago, IL, 10–13 August 2009; received 20 September 2009; revision received 12 December 2009; accepted for publication 14 December 2009.

*Guidance and Control Engineer; ronenat@zahav.net.il.
†Research Fellow; georgeh@rafael.co.il.
‡Research Fellow; haimw@rafael.co.il.
§Senior Lecturer, Faculty of Aerospace Engineering; tal.shima@technion.ac.il. Associate Fellow AIAA.

state estimation is essential. The quality of the target state estimator (TSE) is of prime importance as its outputs drive the guidance law. The most well-known and common linear estimator is the Kalman filter (KF). Basic estimation definitions and concepts are elaborated in [4]. For a linear system and Gaussian noise, the KF is the optimal estimator in the sense of minimum mean square error. For a nonlinear system or nonlinear observations, the extended Kalman filter (EKF) approach may be used. The EKF continuously updates a linearization around the current state estimate.

When the assumed target maneuver and observation noise statistics differ from the actual ones, the performance of the Kalman filter is degraded. One way of overcoming this disadvantage is a method known as the multiple-model (MM) approach. If the target acceleration may be assumed to follow one of several models, then processing the observations using *all* possible models simultaneously, and subsequently using a weighted average of the resulting estimates, is in fact an optimal estimator structure. Magill [5] was the first to introduce such a scheme: the multiple-model adaptive estimation (MMAE) method.

The MMAE assumes that the system is in one of a finite number of modes. The models can differ in the process noise level (its variance), a deterministic output, and/or any other parameter. Each filter's estimate is weighted through the filter's weighting coefficient to form the full multiple-model filter's estimate. The weighting coefficients are a function of the measurements available up to the current time. Sims and Lainiotis [6] further improved the weighting coefficient calculation algorithm to be in a recursive form. Shima et al. [7] presented a computationally efficient MMAE to be used in a missile interception scenario.

The obvious disadvantage of the MMAE scheme is the fact that, to describe real-world guidance systems, the estimator is usually required to contain a large number of filters describing all the possible system modes. In [4], other common multiple-model estimation methods denoted as generalized pseudo Bayesian and interacting multiple model (IMM) are presented, creating a reasonable approximation with only a few filters, usually by truncating old filters' history. A recent paper [8] suggests another approximation for the MMAE scheme, named the temporal multiple-model (TMM) estimator, with the important addition of input estimation.

An important issue of any TSE is the assumed target model, the simplest of which represents the target acceleration as a white noise process. Commonly used is the shaping filter method of [9], in which the target's random behavior is represented by an equivalent linear system for which the first- and second-order statistics match those of the actual stochastic process. One such example is the Singer model [10], in which the target's acceleration is approximated by a first-order Gauss–Markov model, also known as the exponentially correlated acceleration model. In the present work, the target acceleration model is based on [8].

Pursuer acceleration saturation is another major source of increased miss distance. Increasing the penalty on the control effort in the cost function might mitigate the effect or postpone reaching it, but it compromises the guidance performance. In [11], another possibility to postpone saturation is presented, penalizing the state and not just the control in the running cost.

Saturation brings about another important issue for the estimator-guidance scheme; the generally assumed certainty equivalence principle (CEP) seems to be not valid for a limited acceleration control missile, as suggested by [12]. The certainty equivalence principle [13] states that the optimal control law for a stochastic control problem is the optimal control law for the associated deterministic problem, for which the known states are replaced by the estimated ones. This was proved for a linear quadratic Gaussian optimal control problem with unbounded controls. When the CEP holds, it is possible to design an estimator and a control law independently of each other. In this case, the control law may be designed on the basis of deterministic states. This scheme is usually referred to as separation of estimation and control.

When the CEP is not valid (as seems to be the case for realistic guidance problems [12]), it was proved [14] that (for guidance-type information pattern problems) the estimator may be designed independently of the control problem, but the optimal controller depends on the statistics of the estimated state. This principle is known as the one-way separation or general separation theorem (GST). It was used in a recent paper [15] to suggest a novel approach for saturation inclusion in the guidance law. This new linear guidance law named saturated OGL (SOGL), describes saturation using the random input describing function (RIDF) method and solves the stochastic controller problem. This unique formulation results in a guidance law gain that depends on the estimated state statistics. Hexner et al. [15] provided the basis for the guidance law used in the current work. A later work [16] proposed the optimal nonlinear solution for this problem by numerically solving the stochastic optimization problem.

Another noteworthy contribution to the inclusion of the estimator effects on the guidance law is [17], in which the pure delay caused by the estimation process is taken into account in the guidance law. A new approach to fusion of estimation and guidance, under the guidelines of the GST, was recently proposed in [18]. Formulated in a discrete-time setting, particle filtering was used to approximate the entire state conditional probability density function using the exact nonlinear dynamic models without constraining the analysis to the standard Gaussian noise assumptions. Shaviv and Oshman [18] presented a new guidance law that takes into account the conditional probability density function resulting from this estimator.

It is possible to combine an MMAE output state estimate to a single controller (guidance law), as is demonstrated in [7]. When certainty equivalence is not valid, a separate guidance law should be constructed for each estimator, as demonstrated in [19], wherein the initial part of the scenario is devoted to the model identification, after which one filter-guidance law branch is selected. In [20] one may find a concise explanation of the difficulties of combining a multiple-model estimator with a guidance law, when certainty equivalence does not hold. Rusnak [20] used the suboptimal multiple-model adaptive control (MMAC) scheme, which degenerates to an MMAE estimator and the APN guidance law for the specific case shown. Both [7,20] demonstrated the superiority of the MM estimation over a single estimator based on a shaping filter, with the cost of extra computational load, which nowadays may be perfectly feasible. Naturally, Shaviv and Oshman [18], using the particle filter estimator, also fall into the category of combining an MM estimator and a GST-oriented guidance law, with the expense of heavy computational load.

The current work uses the mechanism to identify a sudden target maneuver jump from [8] and the method of development of the guidance law from [15]. This unique combination generates a guidance system that takes into account the pursuer–evader maneuverability ratio and the pursuer's acceleration saturation, in addition to the statistics of the estimated states. The derivation of the guidance law proceeds in two stages. In the first simplified stage, it is assumed that the instance that the target issues a step command in its acceleration is known. However, the size of the target maneuver jump must still be estimated. In the second stage, it is assumed that the target performs a single step maneuver at an unknown time near intercept. A suboptimal guidance law is derived using the MMAC formulation, making this estimation-dependent guidance law adaptive to the target's maneuver with a gain varying according to the current estimated state error statistics.

The remainder of this paper is organized as follows. The next section depicts the problem formulation, the model used, the assumptions, and the available measurements. Next is the solution for a single estimator element matched to the new guidance law and a preliminary performance evaluation. This is followed by an MMAC-type solution, results analysis, and conclusions. The Appendix provides details regarding the solution of the associated two-point boundary value problem (TPBVP).

II. Problem Formulation

The dynamic model of the problem is constructed using the following assumptions: 1) the missile–target engagement occurs in one plane, 2) the missile (pursuer) and the target may be represented by a point mass model with linear dynamics, 3) the relative endgame trajectory is linearized about a fixed reference line (the initial LOS direction), 4) the missile's and the target's speeds remain constant, 5) the missile acceleration is bounded, 6) the missile and the target are modeled as first-order dynamic systems, and 7) the missile acquires noisy measurement of some state variables.

Figure 1 shows the linearized endgame geometry used in our formulation. Here, the X axis is aligned with the initial LOS direction, r is the range between the missile and the target, and φ is the angle between the current and initial LOS. y is the relative displacement, perpendicular to the initial LOS, between the target and the missile and a_T and a_M are the accelerations normal to the initial LOS.

The proposed target model for the estimator is a first-order system, represented by a time constant τ_T, and noise. The deterministic part (first-order system) of the target model is depicted by

$$\frac{a_T}{a_{T_c}} = \frac{1}{1+\tau_T s} \tag{1}$$

For a constant acceleration command, the general target dynamics are described by

$$\begin{cases} \dot{y}_T = v_T \\ \dot{v}_T = a_T \\ \dot{a}_T = -\frac{1}{\tau_T} a_T + \frac{1}{\tau_T} a_{T_c} + \frac{1}{\tau_T} w_T \\ \dot{a}_{T_c} = 0 \end{cases} \tag{2}$$

where y_T, v_T, and a_T are the target's position, velocity, and acceleration, respectively; a_{T_c} is the target's acceleration command; and w_T is a white noise process, representing target acceleration uncertainties (small, possibly random, changes as would result from wind gusts, turbulence, target flight control effects, etc.). All are perpendicular to the initial LOS direction.

The acceleration command satisfies the following assumptions: 1) the acceleration command is a single step function, and 2) the magnitude of the step command is taken from a Gaussian distribution.

The state used in this problem consists of the relative position and velocity, missile acceleration, target acceleration, and target acceleration command (all are perpendicular to the initial LOS direction):

$$\mathbf{x} = [\,y \quad \dot{y} \quad a_M \quad a_T \quad a_{T_c}\,]^T \tag{3}$$

The missile is modeled as a first-order dynamic system with a time constant τ_M, that is, having the following acceleration transfer function:

$$\frac{a_M}{u} = \frac{1}{1+\tau_M s} \tag{4}$$

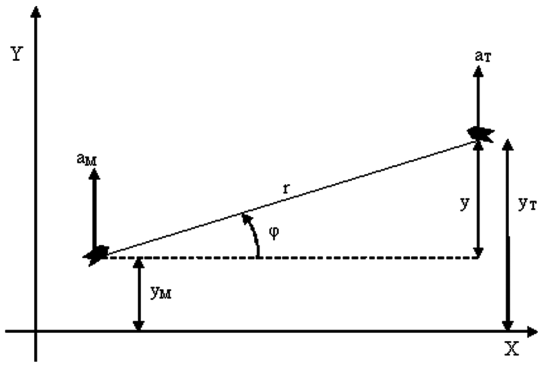

Fig. 1 Linearized endgame geometry.

where u is the maneuver command. Because constant closing speed v_c is assumed and the initial range between the missile and the target is r_0, the final intercept time t_f is well approximated by

$$t_f = r_0 / v_c \tag{5}$$

The time to go is defined as

$$t_{\text{go}} \triangleq t_f - t \tag{6}$$

and the normalized time to go is

$$\theta \triangleq t_{\text{go}} / \tau_M \tag{7}$$

The bounded control will be described as a standard saturation function

$$\text{sat}\,(u) = \begin{cases} U_m & \text{if } u > U_m \\ u & \text{if } -U_m \le u \le U_m \\ -U_m & \text{if } u < -U_m \end{cases} \tag{8}$$

where in our problem $U_m = a_{M_{\max}}$, the missile's maximal maneuver capability.

The equation of motion describing the investigated one-dimensional engagement (perpendicular to the initial LOS) is

$$\dot{\mathbf{x}} = \mathbf{A}\mathbf{x} + \mathbf{b}\,\text{sat}(u) + \mathbf{G}\omega; \qquad \mathbf{x}(0) = \mathbf{x}_0 \tag{9}$$

where

$$\mathbf{A} = \begin{bmatrix} 0 & 1 & 0 & 0 & 0 \\ 0 & 0 & -1 & 1 & 0 \\ 0 & 0 & -\frac{1}{\tau_M} & 0 & 0 \\ 0 & 0 & 0 & -\frac{1}{\tau_T} & \frac{1}{\tau_T} \\ 0 & 0 & 0 & 0 & 0 \end{bmatrix}; \quad \mathbf{b} = \begin{bmatrix} 0 \\ 0 \\ \frac{1}{\tau_M} \\ 0 \\ 0 \end{bmatrix}; \quad \mathbf{G} = \begin{bmatrix} 0 & 0 \\ 0 & 0 \\ \frac{1}{\tau_M} & 0 \\ 0 & \frac{1}{\tau_T} \\ 0 & 0 \end{bmatrix} \tag{10}$$

and $\omega = [\omega_M, \omega_T]^T$ is a two-dimensional white noise, where ω_M and ω_T are white Gaussian processes, representing the uncertainty in missile and target acceleration. The standard deviation of the missile's acceleration is usually taken to be small (0.1–1 g) and represents the uncertainties of the missile's sensors.

The continuous-time measurement taken by the pursuing missile is

$$z = \varphi + v \simeq \mathbf{c}\mathbf{x} + v \tag{11}$$

where the measurement matrix $\mathbf{c}$ is

$$\mathbf{c} = [\,1/r \quad 0 \quad 0 \quad 0 \quad 0\,] \tag{12}$$

and v is the angle measurement error, modeled as a continuous-time white Gaussian noise with spectral density V:

$$V = \sigma_\phi^2 \tag{13}$$

(For discrete-time measurements taken every T_s seconds with variance $\sigma_{\phi_d}^2$, $\sigma_\phi^2 = \sigma_{\phi_d}^2 T_s$.) The range r is assumed to be measured accurately. The cost function to be minimized is

$$J = E\left[\mathbf{x}_\mathbf{f}^\mathbf{T}\mathbf{S}_\mathbf{f}\mathbf{x}_\mathbf{f} + \int_0^{t_f} (\mathbf{x}^\mathbf{T}\mathbf{Q}\mathbf{x} + Ru^2)\,\mathrm{d}t\right] \tag{14}$$

where the subscript f denotes the value at the final time.

For our interception problem, the following matrices are chosen

$$\mathbf{S}_\mathbf{f} = \begin{bmatrix} s_f & 0 & 0 & 0 & 0 \\ 0 & 0 & 0 & 0 & 0 \\ 0 & 0 & 0 & 0 & 0 \\ 0 & 0 & 0 & 0 & 0 \\ 0 & 0 & 0 & 0 & 0 \end{bmatrix}; \quad \mathbf{Q} = \begin{bmatrix} 0 & 0 & 0 & 0 & 0 \\ 0 & 0 & 0 & 0 & 0 \\ 0 & 0 & 0 & 0 & 0 \\ 0 & 0 & 0 & 0 & 0 \\ 0 & 0 & 0 & 0 & 0 \end{bmatrix} \tag{15}$$

making the weighting coefficients, s_f and R, design parameters of the problem.

III. Single Element Estimator-Controller Formulation

The problem of estimating a sudden target step maneuver during the intercept at time-to-go values equal to several missile time constants is a very practical and difficult one. This is the time span in which a large portion of the miss distance is formed. The problem gets more complicated when the pursuing missile's acceleration is bounded, causing another growth in the miss distance. Knowing these two elements' contribution to the guidance performance degradation, we wish to take advantage of the special attributes of the TMM estimator of [8] and the saturation inclusion in the guidance law of [15] to deal with these two major problems in the guidance system. The elemental estimator of [8] is an estimator tuned for a known-time target step acceleration maneuver, and the maneuver magnitude is assumed to be of a Gaussian distribution. This single elemental estimator will be referred to here as a single element TMM estimator.

This section describes a single TMM-type element estimator matched to a target acceleration step of known magnitude distribution at a known time. Subsequently, this estimator will be combined with the SOGL algorithm to create the guidance law (using the one-way separation). It is noteworthy that the single element TMM estimator is the optimal estimator for the assumed target model, and the SOGL will be matched exactly to this optimal estimator. This combination will yield the best available performance such a pair can achieve.

A. Single Element Temporal Multiple-Model Estimator Equations

The derivation of the estimator equations follows [8]. The initial statistics of the estimated state vector $\hat{\mathbf{x}}$ are

$$E[\hat{\mathbf{x}}(0)] = \hat{\mathbf{x}}_{\mathbf{0}} \tag{16}$$

$$E[\hat{\mathbf{x}}(0)\hat{\mathbf{x}}^T(0)] = \mathbf{P}^{\mathbf{0}}_{\hat{\mathbf{x}}\,\hat{\mathbf{x}}} \tag{17}$$

The estimation error, denoted as $\mathbf{e}$, is defined by

$$\mathbf{e} = \hat{\mathbf{x}} - \mathbf{x} \tag{18}$$

Assuming that $\hat{\mathbf{x}}_{\mathbf{0}}$, $\omega(t)$, and $v(t)$ are independent and using Eq. (9), we obtain the following continuous-time filter equations:

$$\dot{\hat{\mathbf{x}}} = \mathbf{A}\hat{\mathbf{x}} + \mathbf{b}\,\mathrm{sat}(u) + \mathbf{k_f}(z - \mathbf{c}\hat{\mathbf{x}}) \tag{19}$$

$$\mathbf{k}_{\mathbf{f}} = \mathbf{P_{ee}}\mathbf{c}^{\mathbf{T}}V^{-1} \tag{20}$$

$$\dot{\mathbf{P}}_{\mathbf{ee}} = \mathbf{A}\mathbf{P_{ee}} + \mathbf{P_{ee}}\mathbf{A}^{\mathbf{T}} - \mathbf{P_{ee}}\mathbf{c}^{\mathbf{T}}V^{-1}\mathbf{c}\mathbf{P_{ee}} + \mathbf{G}\mathbf{G}^{\mathbf{T}}; \qquad \mathbf{P_{ee}}(\mathbf{0}) = \mathbf{P}^{\mathbf{0}}_{\mathbf{ee}} \tag{21}$$

The special feature of the TMM estimator of [8] that allows it to identify sudden target acceleration jumps lies in the estimator initialization.

The initialization includes two operations: 1) initializing the estimator's state vector, and 2) initializing the estimator's error covariance matrix. The state vector is initialized using the best available data at the time of the initialization and setting the fifth state member to $\hat{a}_{T_c} = 0$. The error covariance matrix is initialized by taking the previous value of the 4 by 4 submatrix, forcing p_{55} to the jump uncertainty value σ^2_{jump} and setting remaining elements in the fifth row and column to zero. The setting of the remaining elements in the fifth row and column to zero is due to the fact that the (assumed) new acceleration command is history independent and, hence, uncorrelated to the other state variables. This is shown schematically in Eq. (22) where $(\,)^-$ represents the values before the initialization and $(\,)^+$ the values after:

$$\mathbf{P}^{+}_{\mathbf{ee}} = \begin{pmatrix} p^-_{11} & p^-_{12} & p^-_{13} & p^-_{14} & 0 \\ p^-_{21} & p^-_{22} & p^-_{23} & p^-_{24} & 0 \\ p^-_{31} & p^-_{32} & p^-_{33} & p^-_{34} & 0 \\ p^-_{41} & p^-_{42} & p^-_{43} & p^-_{44} & 0 \\ 0 & 0 & 0 & 0 & \sigma^2_{\text{jump}} \end{pmatrix} \tag{22}$$

Note that this is, in fact, the optimal estimator for the case at hand, when 1) the time of the jump in the target's acceleration command is known, and 2) the target's acceleration step command is uncorrelated with the previous commands.

B. Describing Function Approach

Following [15], the interceptor acceleration saturation will be approximated by an RIDF that is formulated as follows. Let $\varphi(\zeta)$ be an odd single-input–single-output nonlinearity driven by a zero mean Gaussian process ζ. The approximation of $\varphi(\zeta)$ by a linear gain leads to the following minimization problem:

$$\min_L E\{[\varphi(\zeta) - L\zeta]^2\} \tag{23}$$

where L is a RIDF. Let $\varphi(\zeta)$ be the saturation function defined by Eq. (8), where $\zeta = u$. The associated RIDF in this case is given by [21] as

$$L = \mathrm{erf}\left(\frac{U_m}{\sqrt{2}\sigma_u}\right) \tag{24}$$

where

$$\mathrm{erf}\,(\eta) = \frac{1}{\sqrt{\pi}}\int_{-\eta}^{\eta} e^{-\Psi^2}\,\mathrm{d}\Psi \tag{25}$$

$$u \sim N(0, \sigma_u^2) \tag{26}$$

Note that L and $1 - L$ represent the probability of not reaching and reaching saturation, respectively [22].

To understand the mechanism of the RIDF and its influence on the closed loop, we examine Fig. 2. In Fig. 2, the x axis is the error function's argument $U_m/\sqrt{2}\sigma_u$ as appears in Eq. (24) and the y axis is the RIDF's equivalent gain L. σ_u represents the range of values of the control signal in the closed-loop system (due to state uncertainties), and the following is observed:

1) If the standard deviation of the acceleration command approaches zero, the argument increases and the gain L approaches 1, meaning the saturation is inactive.

2) If the standard deviation of the acceleration command rises, in the stochastic case, the argument decreases and the gain L drops to values lower than 1, inducing an attenuation factor, simulating the effect of saturation in the closed-loop system.

Using the RIDF concept, we wish to obtain the optimal linear controller such that

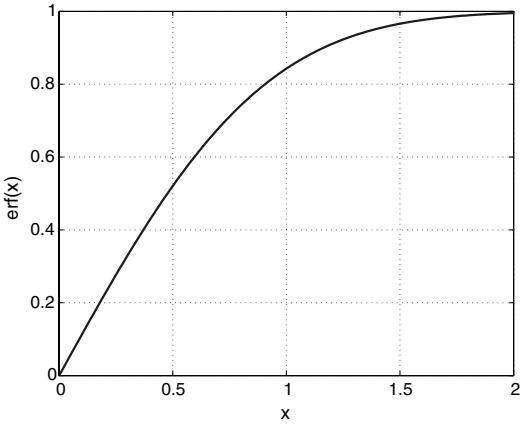

Fig. 2 Error function (erf).

$$u = \mathbf{k_c}\hat{\mathbf{x}} \tag{27}$$

Calculating the control signal variance yields

$$\sigma_u^2 = \mathbf{k_c}\mathbf{P}_{\hat{\mathbf{x}}\hat{\mathbf{x}}}\mathbf{k_c^T} \tag{28}$$

The calculation of the covariance matrix $\mathbf{P}_{\hat{\mathbf{x}}\hat{\mathbf{x}}}$ is based on the approximation of the saturation nonlinearity by the RIDF. It has been shown in [22] that, in the closed-loop system, the replacement of the nonlinearity by an equivalent RIDF produces a reasonable approximation of the relevant statistics.

Using Eqs. (9), (24), and (27)

$$\dot{\hat{\mathbf{x}}} = (\mathbf{A} + L\mathbf{b}\mathbf{k_c})\hat{\mathbf{x}} + \mathbf{k_f}(z - \mathbf{c}\hat{\mathbf{x}}) \tag{29}$$

is obtained. Because $\nu = z - \mathbf{c}\hat{\mathbf{x}}$ is the innovation sequence

$$E[\nu(t)\nu^T(\tau)] = V\delta(t-\tau) \tag{30}$$

we can write the state covariance differential equation as

$$\dot{\mathbf{P}}_{\hat{\mathbf{x}}\hat{\mathbf{x}}} = (\mathbf{A} + L\mathbf{b}\mathbf{k_c})\mathbf{P}_{\hat{\mathbf{x}}\hat{\mathbf{x}}} + \mathbf{P}_{\hat{\mathbf{x}}\hat{\mathbf{x}}}(\mathbf{A} + L\mathbf{b}\mathbf{k_c})^T + \mathbf{k_f}V\mathbf{k_f^T};$$
$$\mathbf{P}_{\hat{\mathbf{x}}\hat{\mathbf{x}}}(\mathbf{0}) = \mathbf{P}^{\mathbf{0}}_{\hat{\mathbf{x}}\hat{\mathbf{x}}} \tag{31}$$

C. Saturated Optimal Guidance Law Built for a Single Temporal Multiple-Model Element Estimator

After the estimator has been formulated and the error covariance matrix is known for the entire scenario duration, the optimal guidance law may be calculated using the one-way separation principle.

The cost function to be minimized is given by

$$\begin{aligned} J &= E\left[\mathbf{x_f^T}\mathbf{S_f}\mathbf{x_f} + \int_0^{t_f}(\mathbf{x^T}\mathbf{Q}\mathbf{x} + Ru^2)\,\mathrm{d}t\right] \\ &= tr[(\mathbf{P}^{\mathbf{f}}_{\hat{\mathbf{x}}\hat{\mathbf{x}}} + \mathbf{P}^{\mathbf{f}}_{\mathbf{ee}})\mathbf{S_f}] \\ &\quad + \int_0^{t_f}(tr[(\mathbf{P}_{\hat{\mathbf{x}}\hat{\mathbf{x}}} + \mathbf{P_{ee}})\mathbf{Q}] + R\mathbf{k_c}\mathbf{P}_{\hat{\mathbf{x}}\hat{\mathbf{x}}}\mathbf{k_c^T})\,\mathrm{d}t \end{aligned} \tag{32}$$

where the minimization is performed with respect to $\mathbf{k_c}$, subject to Eq. (31). Note that $\mathbf{P_{ee}}$ does not depend on $\mathbf{k_c}$ (the one-way separation principle) and the problem to be solved is

$$\min_{\mathbf{k_c}}\left\{tr(\mathbf{P}^{\mathbf{f}}_{\hat{\mathbf{x}}\hat{\mathbf{x}}}\mathbf{S_f}) + \int_0^{t_f}[tr(\mathbf{P}_{\hat{\mathbf{x}}\hat{\mathbf{x}}}\mathbf{Q}) + R\mathbf{k_c}\mathbf{P}_{\hat{\mathbf{x}}\hat{\mathbf{x}}}\mathbf{k_c^T}]\,\mathrm{d}t\right\} \tag{33}$$

subject to Eq. (31), where

$$L = \mathrm{erf}\left(\frac{U_m}{\sqrt{2\mathbf{k_c}\mathbf{P}_{\hat{\mathbf{x}}\hat{\mathbf{x}}}\mathbf{k_c^T}}}\right) \tag{34}$$

Following [22], the Hamiltonian associated with this problem is

$$\begin{aligned} H &= [tr(\mathbf{P}_{\hat{\mathbf{x}}\hat{\mathbf{x}}}\mathbf{Q}) + R\mathbf{k_c}\mathbf{P}_{\hat{\mathbf{x}}\hat{\mathbf{x}}}\mathbf{k_c^T}] + tr\{[(\mathbf{A} + L\mathbf{b}\mathbf{k_c})\mathbf{P}_{\hat{\mathbf{x}}\hat{\mathbf{x}}} \\ &\quad + \mathbf{P}_{\hat{\mathbf{x}}\hat{\mathbf{x}}}(\mathbf{A} + L\mathbf{b}\mathbf{k_c})^T + \mathbf{k_f}V\mathbf{k_f^T}]\mathbf{S}\} \\ &\quad + \lambda\left[\mathbf{k_c}\mathbf{P}_{\hat{\mathbf{x}}\hat{\mathbf{x}}}\mathbf{k_c^T} - \frac{U_m^2}{2[\mathrm{erf}^{-1}(L)]^2}\right] \end{aligned} \tag{35}$$

where the symmetric matrix $\mathbf{S}$ and the scalar λ are Lagrange multipliers. The optimal solution is obtained by solving the following equations:

$$\frac{\partial H}{\partial \mathbf{k_c}} = 0 \tag{36}$$

$$\dot{\mathbf{S}} = -\frac{\partial H}{\partial \mathbf{P}_{\hat{\mathbf{x}}\hat{\mathbf{x}}}} \tag{37}$$

and the transversality condition

$$\mathbf{S}(t_f) = \mathbf{S_f} \tag{38}$$

Observe that L is also an optimization variable under the constraint of Eq. (34); thus,

$$\frac{\partial H}{\partial L} = 0 \tag{39}$$

Equation (36) leads to the relation

$$\mathbf{k_c} = -\frac{L}{R+\lambda}\mathbf{b^T}\mathbf{S} \tag{40}$$

and substituting Eq. (40) into Eq. (34) yields

$$\left(\frac{L}{R+\lambda}\right)^2\mathbf{b^T}\mathbf{S}\mathbf{P}_{\hat{\mathbf{x}}\hat{\mathbf{x}}}\mathbf{S^T}\mathbf{b} = \frac{U_m^2}{2[\mathrm{erf}^{-1}(L)]^2} \tag{41}$$

Equations (37) and (38) are equivalent to the following differential equation:

$$\dot{\mathbf{S}} = -\mathbf{Q} - \mathbf{A^T}\mathbf{S} - \mathbf{S}\mathbf{A} + \frac{L^2}{R+\lambda}\mathbf{S}\mathbf{b}\mathbf{b^T}\mathbf{S}; \qquad \mathbf{S}(t_f) = \mathbf{S_f} \tag{42}$$

Equation (39) is used to derive an expression of λ in terms of L:

$$\lambda = \frac{R}{\frac{\sqrt{\pi}}{2}L\frac{\exp\{[\mathrm{erf}^{-1}(L)]^2\}}{\mathrm{erf}^{-1}(L)} - 1} \tag{43}$$

Equation (41) can be rewritten as

$$\sqrt{\mathbf{b^T}\mathbf{S}\mathbf{P}_{\hat{\mathbf{x}}\hat{\mathbf{x}}}\mathbf{S}\mathbf{b}} = \frac{R+\lambda}{L}\frac{U_m}{\sqrt{2}\mathrm{erf}^{-1}(L)} \tag{44}$$

Substituting Eq. (43) into Eq. (44), we obtain

$$\sqrt{\mathbf{b^T}\mathbf{S}\mathbf{P}_{\hat{\mathbf{x}}\hat{\mathbf{x}}}\mathbf{S}\mathbf{b}} = \frac{R + \frac{R}{\frac{\sqrt{\pi}}{2}L\frac{\exp\{[\mathrm{erf}^{-1}(L)]^2\}}{\mathrm{erf}^{-1}(L)} - 1}}{L}\frac{U_m}{\sqrt{2}\mathrm{erf}^{-1}(L)} \tag{45}$$

The details for solving this optimization problem and the associated TPBVP may be found in [15] and are also repeated in the Appendix.

Equations (40) and (42) induce the following guidance law's structure:

$$u = a_C = \frac{N'_{\mathrm{SOGL}}(t_{\mathrm{go}})}{t_{\mathrm{go}}^2}\widehat{\mathrm{ZEM}}_{\mathrm{SOGL}} \tag{46}$$

with the navigation gain N'_{SOGL} taken from Eq. (40):

$$N'_{\mathrm{SOGL}}(t_{\mathrm{go}}) = \mathbf{k_c}(t_{\mathrm{go}})t_{\mathrm{go}}^2[1 \quad 0 \quad 0 \quad 0 \quad 0]^T \tag{47}$$

and

$$\begin{aligned} \widehat{\mathrm{ZEM}}_{\mathrm{SOGL}} &= \hat{y} + \hat{\dot{y}}t_{\mathrm{go}} - \hat{a}_M\tau_M^2(e^{-\theta} + \theta - 1) \\ &\quad + \hat{a}_T\tau_T^2(e^{-\theta_T} + \theta_T - 1) - \hat{a}_{T_C}\tau_T^2\left(e^{-\theta_T} + \theta_T - 1 - \frac{1}{2}\theta_T^2\right) \end{aligned} \tag{48}$$

$$\theta_T = t_{\mathrm{go}}/\tau_T \tag{49}$$

From here on, the navigation gain N'_{SOGL} will be referred to simply as N'.

D. Performance Evaluation

To evaluate the potential of the newly proposed estimator-guidance-law pair, a performance evaluation was carried out using a simulation of the one-dimensional engagement (perpendicular to the initial LOS). A discrete-time implementation was chosen, sampled over the sampling period T_s. The scenario's parameters are described in Table 1.

In the scenario described, the target produces an acceleration step at a predefined normalized time (denoted as θ_{jump}), which is varied in

Table 1 Scenario parameters for initial performance evaluation

Parameter	Value
r_0, m	2000
v_c, m/s	1000
σ_{ϕ_d}, rad	2e − 3
T_s, s	0.01
σ_{jump}, m/s^2	60
τ_M, s	0.1
τ_T, s	0.3
$a_{M_{\max}}$, m/s^2	200

steps of 0.1 s during the last second of the scenario. The target generates commands as assumed by the estimator's model, that is, commands a step in acceleration for which the amplitude is chosen from a Gaussian distribution with the known σ_{jump}. For each target jump time, a matched, single TMM element estimator was constructed, inducing the covariance change as in Eq. (22) exactly at the known jump time. Then, the covariance of this single element TMM estimator was fed into the SOGL algorithm, resulting in a matched guidance law gain for this specific element estimator. This estimator-guidance law pair represents the best available match, under our derivation scheme, and leads to a performance bound.

Typical guidance gains are shown in Fig. 3 as a function of the normalized time to go θ for different values of target maneuver times. As expected, the effective navigation gain N' is influenced by the covariance increase of the filter. All N' gains, including that of OGL, converge asymptotically (as $\theta \to \infty$) to 3, the constant gain of PN. When the filter initialization occurs a long time before the intercept ($\theta_{\text{jump}} = 10, 7$) the gain resembles that of the original formulated SOGL as appears in [15]. This resemblance represents the fact that this initialized filter's covariance behavior is close to that of the single filter chosen in [15]. When the initialization is expected to happen exactly at the engagement termination (i.e., $\theta_{\text{jump}} = 0$) the gain is identical to that of the classical OGL, as for this case a nonmaneuvering target is expected. If the target jump is expected to happen close to the terminal time ($\theta_{\text{jump}} = 5, 2$) the covariance increase causes a substantial growth in the N' values for $\theta \in [0.5, 2]$. This illustrates the inherent feature of the SOGL to increase, early in the engagement, the gain when uncertainties rise. In a full functional estimator, this increase in the covariance represents the chance of a target maneuver, which means that an increase in N' would occur when the target performs a jump. This agrees with the common guidance engineering practice of increasing the gain when the target maneuvers. Also, the dependence of the guidance law on the actual scenario is observed, a fact that rules out the validity of the CEP in this case.

1. *Homing Performance*

PN, OGL, and SOGL guidance laws were compared, *all using the same target state estimates* from a single TMM estimator. Hence, the achieved improvement is due solely to the different guidance laws used. For each jump time, 100 Monte Carlo runs were simulated and the rms of the miss distance was calculated.

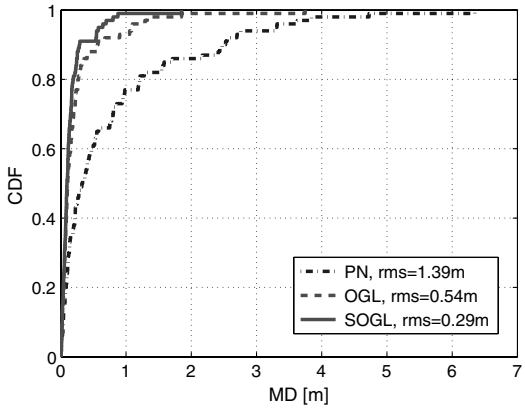

Fig. 4 Sample CDF for target maneuver at $\theta_{\text{jump}} = 7$, $\sigma_{\text{jump}} = 60$ [m/s^2].

Figure 4 shows a sample miss-distance (MD) cumulative distribution function (CDF) for a target maneuvering at $\theta = 7$. The superiority of SOGL over OGL and PN is evident. For example, when using SOGL, in 90% of the cases the miss distance was smaller than about 0.25 m, whereas for OGL and PN it was lower than about 0.5 and 2.5 m, respectively. In the comparisons to follow, we will use the RMS of the MD from the 100 runs when using the different guidance laws. Here it was 0.29, 0.54, and 1.39 m when using SOGL, OGL, and PN, respectively. Figure 5 shows the rms MD obtained from 100 Monte Carlo runs for each target maneuver time. In Fig. 5, a line representing PN performance is included to emphasize the substantial difference between PN, OGL, and SOGL. In all comparisons similar PN behavior was observed, and so, to show the comparable difference between OGL and SOGL, only these two will be presented in the figures to follow.

An examination of Fig. 5 shows typical behavior: little to no improvement occurs in the vicinity of $\theta_{\text{jump}} = 10$. Most of the improvement appears around $\theta_{\text{jump}} = 5, 6, 7$ (about 30%), and from $\theta_{\text{jump}} = 3$ and on, OGL and SOGL performance coincide. Note that $\theta_{\text{jump}} = 0$ represents the case of a nonmaneuvering target.

The behavior at $\theta_{\text{jump}} = 10$ is explained by the fact that both OGL and SOGL have enough time to close the ZEM and obtain a similar miss distance. Also, by examining Fig. 3 it is obvious that SOGL's N' for target jumps in this region resembles that of the ordinary OGL. The region of $\theta_{\text{jump}} = 5, 6, 7$ is where most improvement is observed. This is expected because this is the region where N' of SOGL is significantly different from that of the ordinary OGL. This is the region in which, if a target maneuvered and the maneuver were properly identified, it would be wise for the pursuer to apply as much acceleration command as possible to null the ZEM. SOGL's higher gain does just that. The region of $\theta_{\text{jump}} \in [0, 4]$ is characterized by the

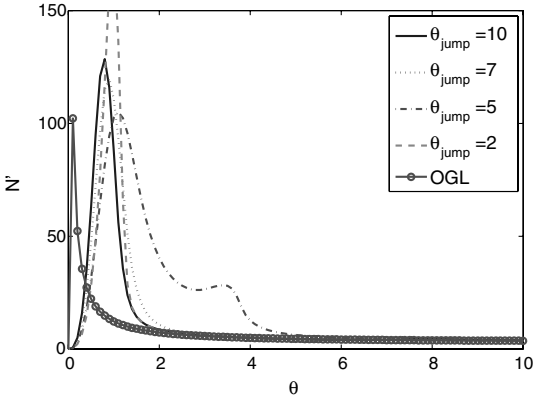

Fig. 3 Sample SOGL guidance gains.

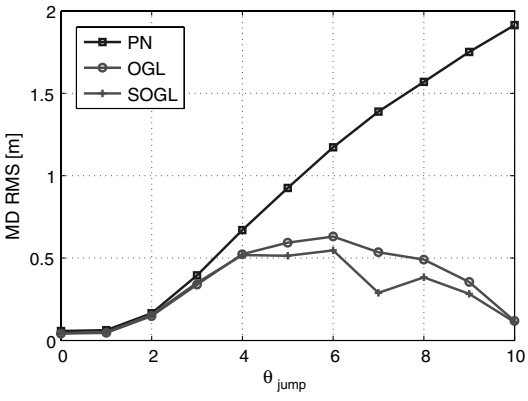

Fig. 5 The rms miss distance vs θ_{jump}, $\sigma_{\text{jump}} = 60$ [m/s^2].

Table 2 Angular noise measurement values and their definitions in graphs

Angular noise level—σ_{ϕ_d}, mrad	Definition in graphs
0.5	Low
1	Med
2	Hi

Table 3 Expected target maneuver magnitude values and their definitions in graphs

Expected target maneuver magnitude—σ_{jump}, m/s^2	Definition in graphs
40	Low
60	Med
90	Hi

fact that both OGL and SOGL (and, from $\theta_{\text{jump}} = 2$, PN) gains are high enough to saturate the acceleration command (as N' is divided by t_{go}), so that the performance of SOGL and OGL are similar. It is important to understand that the extra information used in SOGL (the covariance enlargement) is of no use to the conventional OGL and does not change its structure or behavior; thus, OGL is the reasonable comparison basis for SOGL.

2. *Gains Sensitivity to Noise Level*

For a matched estimator SOGL, the only difference between OGL and SOGL lies in the different behavior of the guidance gain N'. This fact implies that, by exploring the behavior of N' with some varying parameters, we will gain better understanding of this guidance system and its expected behavior.

In this section, we wish to explore the varying behavior of the guidance gain N' when the angular measurement noise level changes. The scenario parameters are defined in Table 1 with the varying angular measurement noise as defined in Table 2.

For the sake of clarity, and to deliver only the important details, the labels of the axes were removed from the figure and are elaborated as follows: 1) the horizontal x axis is the normalized time to go θ, 2) the vertical y axis is the guidance gain N', and 3) each graph's title represents the corresponding θ in which a jump had occurred and for which the estimator-guidance-law pair was constructed.

The gains shown in Fig. 6, which corresponds to target jump times of $\theta = 9, 8, 7, \ldots, 1$, are the gains for which most of the important phenomena may be observed:

1) As observed before, a short time after a filter has been initialized, the gain increases. This increase in N' grows larger with the increase in noise level. The phenomenon is best observed in $\theta_{\text{jump}} = 4, 5$. This is the SOGL's reaction to an increase in the estimation statistics uncertainties due to larger measurement noise. A similar effect has already been shown in [15], with the important difference of being constructed with a different type of estimator.

2) The increase in measurement noise causes the gains to rise earlier in the last few missile time constants of the intercept. Again, this represents the SOGL's feature of increasing the gain when uncertainties rise and saturating the missile's acceleration command earlier in the scenario. This, too, was demonstrated in [15]. The phenomenon is best observed in $\theta_{\text{jump}} = 7, 8, 9$. Both effects represent the physical and common engineering practice of increasing the gain when uncertainties in the expected ZEM values increase, to react fast to a possible target maneuver.

Note that the high values of the navigation gain shown in Fig. 6 serve to saturate the guidance command for relatively small values of ZEM. The value of the guidance gain primarily influences the specific value of ZEM required to saturate the guidance command.

3. *Gains Sensitivity to Expected Target Maneuver Magnitude*

In this section, we wish to explore the varying behavior of the guidance gain N' when the expected target maneuver magnitude changes. The scenario parameters are defined in Table 1 with the varying expected maneuver magnitude σ_{jump} as defined in Table 3.

Again, for the sake of clarity and to deliver only the important details, the labels of the axes were removed from the figure and are elaborated as follows: 1) the horizontal x axis is the normalized time to go θ, 2) the vertical y axis is the guidance gain N', and 3) each graph's title represents the corresponding θ in which a jump had occurred, and for which the estimator-guidance-law pair was constructed.

The gains shown in Fig. 7 which corresponds to target jump times of $\theta = 9, 8, 7, \ldots, 1$, are the gains with which most of the important phenomena may be observed:

1) As observed before, a short time after a filter has been initialized, the gain increases. This increase in N' grows larger with the increase in expected target maneuver magnitude. The phenomenon is best observed in $\theta_{\text{jump}} = 6, 7, 8$. Again, this is the SOGL's reaction to an increase in the estimation statistics uncertainties due to larger expected target maneuver magnitude. This phenomena was not demonstrated in [15] because this is a unique effect caused by our use of a TMM elemental filter and its initialization.

2) The increase in expected target maneuver magnitude causes the gains to rise earlier in the last few missile time constants of the

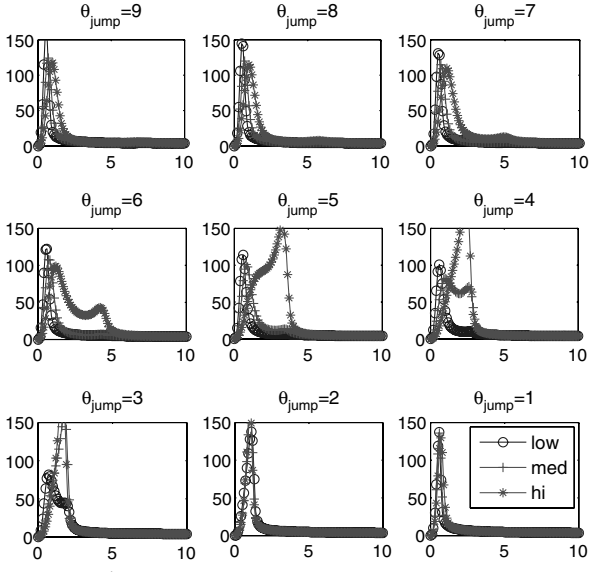

Fig. 6 N' sensitivity to angular measurement noise level σ_{ϕ_d}.

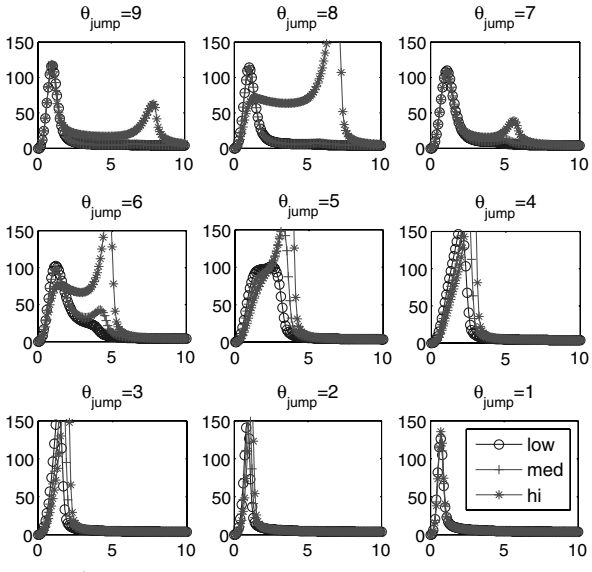

Fig. 7 N' sensitivity to expected target maneuver magnitude σ_{jump}.

intercept. Again, this represents the SOGL's feature of increasing the gain when uncertainties rise, and saturating the missile earlier in the scenario. The phenomenon is best observed in $\theta_{\text{jump}} = 3, 4, 5$.

3) It is observed that the increase in expected target maneuver magnitude does not increase the gain proportionally, but rather causes an abrupt and powerful increase in N'. This is due to the fact that SOGL identifies the expected target maneuver magnitude as being a very large expected ZEM uncertainty, causing a large increase in N' and inducing a saturated pursuer acceleration command as early as possible.

Again, these effects explain the common engineering practice of increasing the gain when uncertainties in the expected ZEM values increase, to react fast to a possible target maneuver.

Here, too, it is noteworthy that the high gains, especially in the last few missile time constants of the intercept and, in this case, even earlier in the scenario, yield a saturating pursuer acceleration command.

IV. Multiple-Model Adaptive Control Approach Solution

In this section, an MMAC scheme is used to construct a feasible implementation of an estimator-guidance-law scheme. In this scheme, the time of the jump in the target's acceleration is no longer assumed to be known. To derive this solution, a brief review of the multiple-model approach is presented, followed by an overview of the MMAC approach principles and the specific suggested MMAC solution for the problem at hand.

A. Multiple-Model Approach

Our approach is based on the use of the MM approach, which is now introduced. In the basic MM approach, it is assumed that the system obeys one of a finite number of models. The filter is constructed using a Bayesian framework. Starting with previous probabilities of each model being correct, the corresponding posterior probabilities are obtained. It is assumed that the model the system obeys is fixed (also referred to as the system mode being fixed) for the entire estimation process and that it is one of the r possible models (the system is in one of r possible modes). Mathematically formulating the above, the system mode M is

$$M \in \{M_j\}_{j=1}^{r} \tag{50}$$

The prior probability that M_j is correct (the system is in mode j) given Z^0 is

$$p\{M_j|Z^0\} = \mu_j(0) \qquad j = 1, \ldots, r \tag{51}$$

where Z^0 is the pior information. Note that

$$\sum_{j=1}^{r} \mu_j(0) = 1 \tag{52}$$

because the correct model is among the assumed r possible models. It is assumed that all models are linear Gaussian.

Using Bayes formula, the posterior probability of model j being correct, given the measurement data up to time k (also referred to as the weighting coefficients), is obtained recursively as

$$\mu_j(k) = p\{M_j|Z^k\} = \frac{p[z(k)|Z^{k-1}, M_j]\mu_j(k-1)}{\sum_{i=1}^{r} p[z(k)|Z^{k-1}, M_i]\mu_i(k-1)} \qquad j = 1, \ldots, r \tag{53}$$

starting the recursive calculation with Eq. (51). The probability appearing in the nominator of Eq. (53) is referred to as the likelihood function of mode j at time k, which, under the linear-Gaussian assumptions, is given by the expression

$$\Lambda_j(k) \triangleq p[z(k)|Z^{k-1}, M_j] = p[\nu_j(k)] \sim N[0, S_j(k)] \tag{54}$$

where ν_j and S_j are the innovation and its covariance from the mode-matched filter corresponding to mode j. A filter matched to each mode is constructed, yielding a *mode-conditioned state estimate* and a *mode-conditioned error covariance*. The probability of each mode being correct is obtained according to Eq. (53) based on its likelihood function (54) relative to the other filters' likelihood functions. This filter structure consists of r linear filters. After the filters are initialized, they run recursively on their own estimates. Their likelihood functions are used to update the mode probabilities. The latest mode probabilities are used to combine the mode-conditioned estimate and covariance for that time. Under these assumptions, the probability density function of the state of the system is a Gaussian mixture with r terms:

$$p[\mathbf{x}(k)|Z^k] = \sum_{j=1}^{r} \mu_j(k) N[\hat{\mathbf{x}}^j(k|k), P_j(k|k)] \tag{55}$$

The combination of the mode-conditioned estimates and covariance is carried out as follows:

$$\hat{\mathbf{x}}(k|k) = \sum_{j=1}^{r} \mu_j(k)\hat{\mathbf{x}}^j(k|k) \tag{56}$$

and

$$\mathbf{P}(k|k) = \sum_{j=1}^{r} \mu_j(k)\{\mathbf{P}^j(k|k) + [\hat{\mathbf{x}}^j(k|k) - \hat{\mathbf{x}}(k|k)][\hat{\mathbf{x}}^j(k|k) - \hat{\mathbf{x}}(k|k)]^T\} \tag{57}$$

Equations (56) and (57) are exact under the following assumptions: 1) the correct model is among the set of models considered, and 2) the same model has been in effect from the initial time.

This multiple-model formulation is usually referred to as the multiple-model adaptive estimation scheme.

B. Multiple-Model Adaptive Control Solution

Multiple-model adaptive control is an approximate (suboptimal) scheme for combining an MMAE-type estimator with an estimator-dependent controller. When the controller is independent of the estimator, it is possible to match the combined output estimate of the MMAE estimator of Magill [5] with a single controller, but this is not the case for our matched estimator-controller pair. In the MMAC scheme, each MMAE-type filter is combined with its matched controller and the controllers outputs are weighted using the same weighting coefficients of the MMAE estimator (53), to form an equivalent control signal for the system's plant. A brief review of the MMAC scheme appears in [13].

Most real-world targets will rarely switch their maneuver direction, type, or magnitude in the last 10 time constants of the interception. At most, a single new maneuver will start at these last instances of the engagements. And any maneuver starting at that time, with a target time constant as assumed here (0.3 s), will appear mostly as a step or some part of it. Therefore, the assumption of a single step occurring in these last 10 time constants is perfectly reasonable and will be used here.

Using the knowledge gained from the initial performance evaluation (Sec. III.D), it is obvious that the combined TMM–SOGL algorithm does not yield a significant improvement if initialized earlier than 10 missile time constants before the intercept time. This is also evident from the almost unchanged N' resulting from initializations before the 10 missile time constants limit. Understanding that the important time span to be dealt with is the last 10 missile time constants, a MMAC-type guidance system structure is formed.

The MMAC system as it appears in Fig. 8 is constructed from 11 filter-guidance law branches (this system will be identified here as "MMAC11F") matched to the 10 possible target jump times of the span obtained in Sec. III.D ($\theta_{\text{jump}} = 10, 9, 8, \ldots, 1$) and another filter

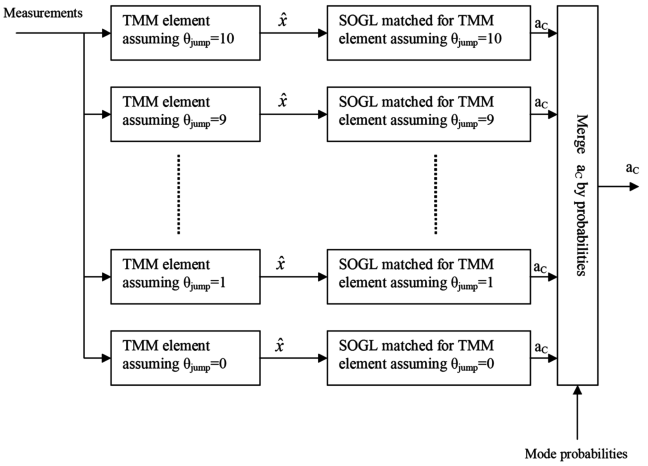

Fig. 8 MMAC11F approach solution.

representing a jump at $\theta_{\text{jump}} = 0$, which is equivalent to a filter representing no target jump at all.

Each of the component models of the multiple-model architecture assumes a jump in the target acceleration command at a known time, but with an unknown magnitude. The jump magnitude is assumed to be *zero mean*, Gaussian distributed, with a known σ_{jump}. In this case, until a jump is identified, the expected value of the target acceleration command remains unchanged, regardless of the known different jump times that are assumed in each of the component models of the multiple-model architecture. That is, a constant acceleration command is assumed for all models. Therefore, all the $\widehat{\text{ZEM}}_{\text{SOGL}_i}$ have identical expressions:

$$\widehat{\text{ZEM}}_{\text{SOGL}_i} = \hat{y}_i + \hat{\dot{y}}_i t_{\text{go}} - \hat{a}_{M_i}\tau_M^2(e^{-\theta} + \theta - 1) + \hat{a}_{T_i}\tau_T^2(e^{-\theta_T} + \theta_T - 1) - \hat{a}_{T_{c_i}}\tau_T^2\left(e^{-\theta_T} + \theta_T - 1 - \frac{1}{2}\theta_T^2\right) \quad (58)$$

Note that, although for all of our MMAC-based guidance laws the ZEM structure is identical, for each different value of i (different model), appropriate values of $\hat{y}_i$, $\hat{\dot{y}}_i$, $\hat{a}_{M_i}$, $\hat{a}_{T_i}$, and $\hat{a}_{T_{c_i}}$ are used.

The MMAC-based control law is

$$a_c = \sum_{i=1}^{11} \mu_i \frac{N_i'(t_{\text{go}})}{t_{\text{go}}^2}\hat{z}_i(t_{\text{go}}) \quad (59)$$

where $\hat{z}_i(t_{\text{go}})$ is the expectation of the zero-effort miss conditioned on the measurements until the current time and on the assumed time t_i of the step in the target acceleration, μ_i is the conditional probability of the target acceleration step occurring at time t_i, and $N_i'(t_{\text{go}})$ is the optimal guidance gain associated with a step in the target acceleration at time t_i of unknown (random) amplitude.

Remark 1: The stochastic target model used in the current work specifies the random behavior of the target acceleration from the beginning of the engagement to intercept time. Consequently, the assumed model dictates the zero-effort-miss calculation. Our model assumes that the target acceleration is the sum of two components: a first-order Gauss–Markov process and a single step in the target acceleration command, occurring at an unknown (random) time. In particular, the ZEM calculation in Eq. (58) shows that, at any instant, the future values of the target acceleration are the sum of the present estimate of the target acceleration ($\hat{a}_{T_i}$) decaying with the assumed target time constant for the Gauss–Markov component and a constant acceleration command ($\hat{a}_{T_{c_i}}$) acting through the assumed target time constant.

Remark 2: If the SOGL is replaced by OGL, then $N_i'(t_{\text{go}}) = N'(t_{\text{go}})$ for all i. In this case, Eq. (59) can be rewritten as

$$a_c = \sum_{i=1}^{11} \mu_i \frac{N'(t_{\text{go}})}{t_{\text{go}}^2}\hat{z}_i(t_{\text{go}}) = \frac{N'(t_{\text{go}})}{t_{\text{go}}^2}\hat{z}_e(t_{\text{go}}) \quad (60)$$

where

$$\hat{z}_e(t_{\text{go}}) = \sum_{i=1}^{11} \mu_i \hat{z}_i(t_{\text{go}}) \quad (61)$$

This was the form of the guidance law in [20], in which this structure was used along with the APN guidance law.

Remark 3: The guidance gains $N_i'(t_{\text{go}})$ of the different models in Eq. (59) can be computed a priori. As is common in the missile guidance community, these gains can then be stored in a lookup table to be used online.

C. Performance Evaluation

1. Comparison to the Bound

To compare the performance with that of the bound obtained in Sec. III.D, the same scenario (see Table 1) will be addressed and two types of target behaviors will be evaluated:

1) A target behaving according to the assumed model, for example, commands a step in acceleration for which the amplitude is chosen from a Gaussian distribution with the known σ_{jump}.

2) A target performing a step with a magnitude of $\pm\sigma_{\text{jump}} = 60$ [m/s^2].

Figure 9 shows the performance in which the target commands a step in acceleration for which the amplitude is chosen from a Gaussian distribution with the known σ_{jump}, that is, acts according to the assumed model. Figure 10 shows the performance in which the target is performing a step with a magnitude of ± 60 [m/s^2], that is, commands a step with a constant value of 60 [m/s^2] with equal probability of its sign.

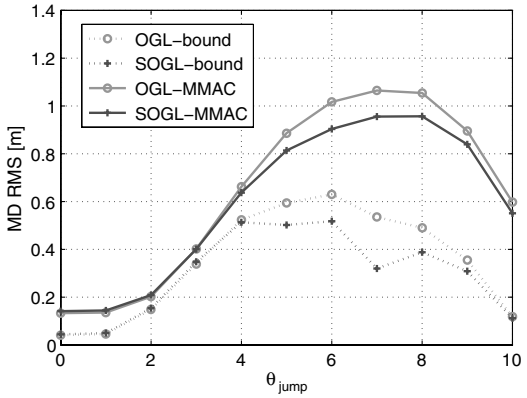

Fig. 9 The rms miss distance vs θ_{jump}, $\sigma_{\text{jump}} = 60$ [m/s^2]. Comparison of MMAC11F with the performance bound.

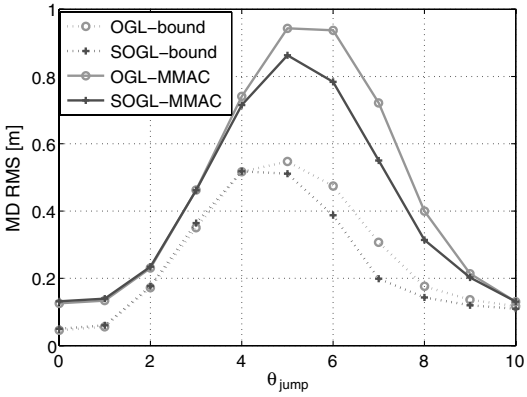

Fig. 10 The rms miss distance vs θ_{jump}, $\sigma_{\text{jump}} = 60$ [m/s^2]. Target jumps $\pm\sigma_{\text{jump}}$. Comparison of MMAC11F with the performance bound.

Figures 9 and 10 reveal the same typical behavior as emerged from Sec. III.D and the same physical explanations apply. It is also obvious that the overall performance degrades substantially. This is expected because the MMAE estimator used (as part of the MMAC scheme) cannot perform as well as a single estimator that knows exactly the jump time. The MMAE estimator has a convergence-to-model time that depends on the measurements delivering enough information to differentiate the actual target maneuver from the noise and to identify the correct model. It should also be noted that, even if the correct model had been selected, it would only be in effect with a probability of 0.95, because a lower probability bound of 0.05 was forced as a minimum bound on all of the MMAE's remaining filters (as a mechanism for preventing one of the filters being "locked" in zero probability and never being able to recover from this probability). This is also a part of the explanation of why, at $\theta = 0$, the performance of the MMAC scheme does not coincide with that of the performance bound.

2. *Sample Run*

The behavior of the MMAE filter is better understood by examining a sample run (Figs. 11 and 12) showing the filter's probabilities and the target's acceleration estimate for a jump time of $t = 1.3$ s, which is equivalent to $\theta = 7$.

The delay caused by the identification of the correct filter causes a delay in selecting the correct SOGL, until the identification is complete. This is another main cause of the large performance degradation between the performance bound and the MMAC11F scheme.

Initiating target jumps between model-matched initialization times (such as $\theta_{\text{jump}} = 5.5$) resulted in smooth behavior of the rms miss-distance line. This is due to the MMAE convergence property to the nearest matched model if the exact model is not present.

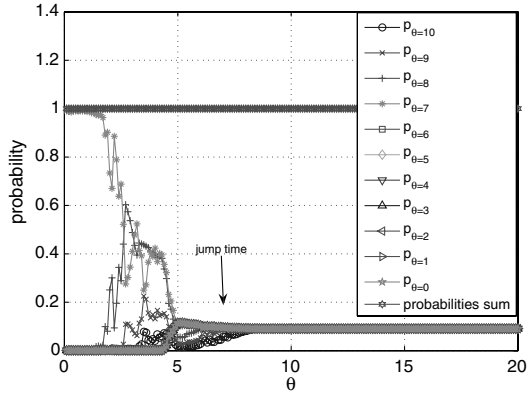

Fig. 11 Probabilities behavior of the MMAC11F for a target jump time of $\theta_{\text{jump}} = 7$, sample run.

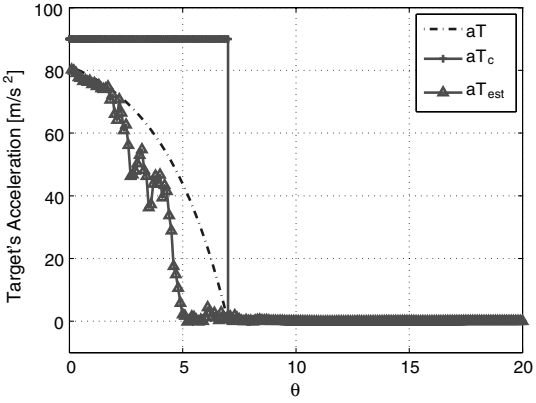

Fig. 12 Target acceleration estimation behavior of the MMAC 11F for a target jump time of $\theta_{\text{jump}} = 7$, sample run.

In summary, the MMAC11F scheme shows a significant improvement of the SOGL over the OGL, keeping the same behavior as observed in the performance bound.

3. *Measurement Noise Level Impact*

In this section, we wish to explore the MMAC11F scheme behavior when the measurement noise level changes. The variations in N', due to this effect, have already been shown in Sec. II, but the actual performance was not evaluated.

Figure 13 presents the performance of the MMAC11F scheme for varying measurement noise levels $\sigma_{\phi_d} = 0.5, 1, 2$ [m rad] and a target performing jumps as assumed by the estimator's model, namely, commanding a step in acceleration for which the amplitude is chosen from a Gaussian distribution with the known σ_{jump}. Figure 14 presents the performance for the same measurement noise variation, only here the target is performing a step with a magnitude of ± 60 [m/s^2].

As expected, in general, performance decreases with the rise in angular measurement noise. The more interesting result is that, as the angular measurement noise increases, the SOGL scheme becomes more effective in improving the absolute rms miss distance. This is expected, recalling that the SOGL gain increases with increasing uncertainty in ZEM. It may be observed in the figures that the absolute improvement for the low measurement noise is much smaller than the improvement reached when the measurement noise level is high.

Examining the maximal improvement percentage over the various noise levels reveals that, in all three examined noise levels, the improvement over OGL is about 20–30%.

Improvement is observed for both the target acting according to the assumed model and with the target (acting more like a real target)

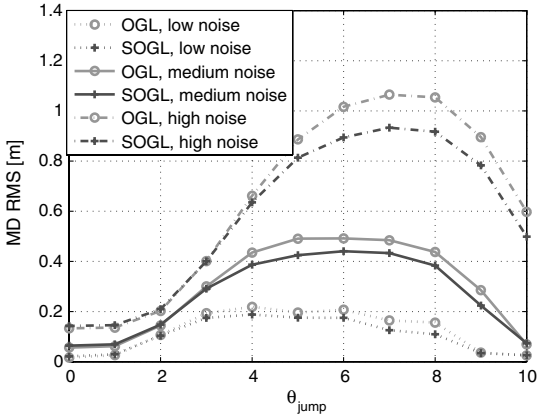

Fig. 13 MMAC11F: rms miss distance vs θ_{jump}, $\sigma_{\text{jump}} = 60$ [m/s^2]. Target behaves as its model. Comparison of noise levels.

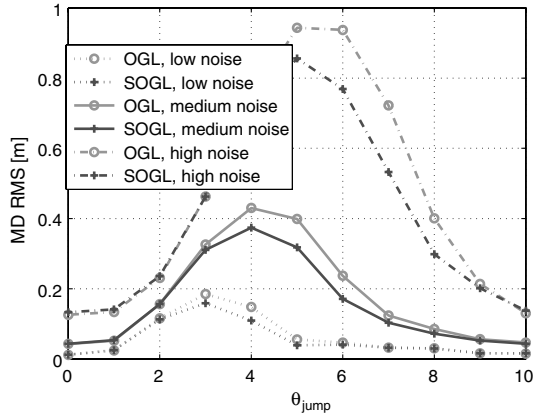

Fig. 14 The rms miss distance vs θ_{jump}, $\sigma_{\text{jump}} = 60$ [m/s^2]. Target jumps $\pm\sigma_{\text{jump}}$. Comparison of noise levels.

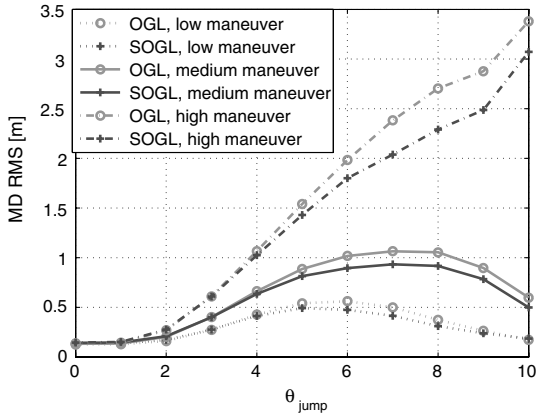

Fig. 15 MMAC11F: rms miss distance vs θ_{jump}, $\sigma_{\text{jump}} = 40, 60, 90$ [m/s^2]. Target jumps with σ_{jump}, Comparison of expected target maneuver effect.

issuing constant step acceleration commands, implying the robustness of this proposed scheme.

4. Expected Target Maneuver Magnitude Impact

In this section, we wish to explore the MMAC11F scheme behavior when the expected target maneuver magnitude changes. The variations in N' due to this effect have already been shown in Sec. III, but the actual performance was not evaluated. Here, we will show the performance of the MMAC11F scheme where the angular noise measurement was taken as constant as $\sigma_{\phi_d} = 2$ [m rad].

Figure 15 presents a comparison between the performance of the OGL with the performance of the new MMAC11 scheme. The performances are presented for three values of the expected value of the target jump amplitude, $\sigma_{\text{jump}} = 40, 60, 90$ [m/s^2], indicated as the low, medium, and high maneuvers in the figure.

Figure 16 presents the performance of MMAC11F for the same expected target maneuver magnitude variation, but with a target performing a step with a magnitude of the assumed $\pm\sigma_{\text{jump}}$.

For all cases examined, the obvious effect of increasing the rms miss distance as the target actual jump magnitude increases may be observed. Again, the more dramatic performance improvement is observed as the target jump magnitude increases. This effect is achieved by the higher gains of the SOGL in the appropriate time spans saturating the pursuer's acceleration command earlier in the scenario. The higher gains are credited to the RIDF that takes into account the saturation as an attenuation factor over the commanded missile acceleration, causing an increase in the required navigation gain.

Examining the maximal improvement percentage over the various expected target maneuver magnitudes reveals the following:

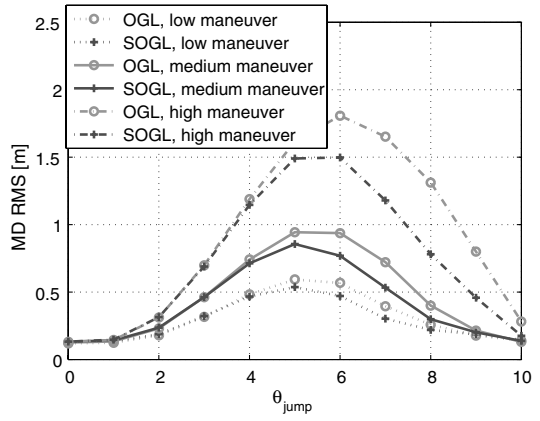

Fig. 16 The rms miss distance vs θ_{jump}, $\sigma_{\text{jump}} = 40, 60, 90$ [m/s^2]. Target jumps $\pm\sigma_{\text{jump}}$. Comparison of expected target maneuver effect.

1) The maximal improvement for the low expected target maneuver magnitude ($\sigma_{\text{jump}} = 40$ [m/s^2]) is about 15–20%.

2) The maximal improvement for the medium expected target maneuver magnitude ($\sigma_{\text{jump}} = 60$ [m/s^2]) is about 25–30%.

3) The maximal improvement for the high expected target maneuver magnitude ($\sigma_{\text{jump}} = 90$ [m/s^2]) is about 40–45%.

These results emphasize the inherent ability of the SOGL to yield better performance than the OGL in scenarios in which pursuer acceleration saturation is expected.

Improvement is observed for both the target acting according to the assumed model and for the target (acting more like a real target) issuing constant step acceleration commands, implying on robustness of this proposed scheme over different scenarios.

V. Conclusions

The endgame scenario of a bounded acceleration missile pursuing a target performing a step maneuver was investigated. A unique single element temporal multiple-model-type estimator was chosen. The estimator was matched with a SOGL, for which the gain depends on the estimated state error covariance.

Performance evaluation was carried out to establish a bound on the best available performance given the investigated scheme of using a random input describing function and a linear guidance law. The results showed an improvement over the deterministic OGL of up to 30% in the rms miss distance for jump times in the last 10 missile time constants. The resulting navigation gain of the new guidance law showed a unique behavior of increasing the effective gain when uncertainties arose and, hence, implementing the usual engineering practice of increasing the gain for a maneuvering target. The improvement was typically in the region of 10 to 3 missile time constants before the intercept time. In the region of the last three missile time constants, before the intercept time, no improvement is observed because both guidance laws have high-enough gains to saturate the missile acceleration command.

A combined multiple-model-based estimator-guidance-law scheme was presented. The adaptive nature of the MMAC scheme results in a target maneuver adaptive guidance law for our acceleration bounded missile. The adaptivity lies in the fact that the guidance law changes its gain according to the target maneuvers and scenario noise uncertainties. In our assumed stochastic target model, the future value of the target acceleration command is its present expected value, conditioned on the observations to the present time. That is, a constant acceleration command is assumed for all models. Therefore, all the ZEM terms have identical expressions. In particular, the ZEM of all the models is independent of the known jump time.

The MMAC-type scheme using 11 filters was constructed for the evaluation of an actual guidance system operational structure and showed a substantial improvement of the SOGL scheme over that of the OGL. Sensitivity analysis to various noise levels and expected target maneuvers was carried out, emphasizing the robustness and advantages of this scheme.

Appendix: Two-Point Boundary Value Problem Solution

The solution for the associated TPBVP appears in [15] and is repeated here for the sake of completeness. The optimal controller equations, derived in Sec. III, constitute a TPBVP. The approach used to solve these equations is essentially the first-order differential dynamic programming (DDP) approach [23]. The solution method is summarized as follows:

1) Solve Eq. (21) and find $\mathbf{P_{ee}}(t)$ for $0 < t < t_f$.

2) Calculate $\mathbf{K_f(t)}$ from Eq. (20) using $\mathbf{P_{ee}}(t)$.

3) Set $L(t) = 1$; $0 < t < t_f$ and $\lambda(t) = 0$; $0 < t < t_f$.

4) Solve Eq. (42) to find $\mathbf{S(t)}$.

5) Calculate $\mathbf{k_c(t)}$ from Eq. (40) using $\mathbf{S(t)}$.

6) Solve Eq. (31) and find $\mathbf{P_{\hat{x}\hat{x}}(t)}$ using $\mathbf{k_c(t)}$ and $\mathbf{k_f(t)}$.

7) Solve Eq. (41) and (43) numerically to find $L(t)$ and $\lambda(t)$ using $\mathbf{S(t)}$ and $\mathbf{P_{\hat{x}\hat{x}}(t)}$.

8) If the change in the cost function is less than 0.1%, the algorithm terminates; otherwise go back to step 4.

Remarks:

1) The initial iteration starts with $L(t) = 1$ and $\lambda(t) = 0$, which represent the linear case without saturation.

2) In all the examples that have been examined, the first-order algorithm has converged. However, if the first-order method fails, the ideas put forward in [23] may be used. It is also possible to use the second-order DDP method to speed up convergence.

3) For ease of calculation and speeding up convergence, the left-hand side of Eq. (45) is evaluated as polynomial, before the iterations, as a function of L and R, knowing that L can vary in the range of $0 < L < 1$ only. During the iterated solution, once the left-hand side of Eq. (45) is known, the values for L and λ can be evaluated directly.

References

[1] Yuan, L., "Homing and Navigational Courses of Automatic Target-Seeking Devices," *Journal of Applied Physics*, Vol. 19, No. 12, 1948, pp. 1122–1128. doi:10.1063/1.1715028

[2] Zarchan, P., *Tactical and Strategic Missile Guidance*, 5th ed., Vol. 219, Progress in Astronautics and Aeronautics, AIAA, Reston, VA, 2007, pp. 143–161.

[3] Cottrell, R. G., "Optimal Intercept Guidance for Short-Range Tactical Missiles," *AIAA Journal*, Vol. 9, No. 7, 1971, pp. 1414–1415. doi:10.2514/3.6369

[4] Bar-Shalom, Y., and Li, X. R., *Estimation and Tracking: Principles, Techniques and Software*, Artech House, Norwood, MA, 1993, pp. 339–414.

[5] Magill, D. T., "Optimal Adaptive Estimation of Sampled Stochastic Processes," *IEEE Transactions on Automatic Control*, Vol. 10, No. 4, 1965, pp. 434–439. doi:10.1109/TAC.1965.1098191

[6] Sims, F. L., and Lainiotis, D. G., "Recursive Algorithm for the Calculation of the Adaptive Kalman Filter Weighting Coefficients," *IEEE Transactions on Automatic Control*, Vol. 14, April 1969, pp. 215–218. doi:10.1109/TAC.1969.1099155

[7] Shima, T., Oshman, Y., and Shinar, J., "Efficient Multiple Model Adaptive Estimation in Ballistic Missile Interception Scenarios," *Journal of Guidance, Control, and Dynamics*, Vol. 25, No. 4, 2002, pp. 667–675. doi:10.2514/2.4961

[8] Hexner, G., Weiss, H., and Dror, S., "Temporal Multiple Model Estimator for a Maneuvering Target," AIAA Paper 2008-7456, 2008.

[9] Zarchan, P., "Representation of Realistic Evasive Maneuvers by the Use of Shaping Filters," *Journal of Guidance, Control, and Dynamics*, Vol. 2, No. 4, 1979, pp. 290–295. doi:10.2514/3.55877

[10] Singer, R. A., "Estimating Optimal Tracking Filter Performance for Manned Maneuvering Targets," *IEEE Transactions on Aerospace and Electronic Systems*, Vol. AES-6, No. 4, 1970, pp. 473–483. doi:10.1109/TAES.1970.310128

[11] Shinar, J., Levinson, S., Weiss, H., and Ben-Asher, J., "Trajectory Shaping in Linear-Quadratic Pursuit-Evasion Games," *Journal of Guidance, Control, and Dynamics*, Vol. 27, No. 6, 2004, pp. 1102–1105. doi:10.2514/1.9765

[12] Shinar, J., and Turetsky, V., "What Happens When Certainty Equivalence Is Not Valid? Is There an Optimal Estimator for Terminal Guidance?," *Annual Reviews in Control*, Vol. 27, No. 2, 2003, pp. 119–130. doi:10.1016/j.arcontrol.2003.10.001

[13] Maybeck, P. S., *Stochastic Models, Estimation, and Control*, Vol. 3, Academic Press, New York/London/Orlando, FL, 1982, pp. 1–62, 253.

[14] Witsenhausen, H. S., "Separation of Estimation and Control for Discrete Time Systems," *Proceedings of the IEEE*, Vol. 59, No. 11, 1971, pp. 1557–1566. doi:10.1109/PROC.1971.8488

[15] Hexner, G., Shima, T., and Weiss, H., "LQG Guidance Law with Bounded Acceleration Command," *IEEE Transactions on Aerospace and Electronic Systems*, Vol. 44, No. 1, 2008, pp. 77–86. doi:10.1109/TAES.2008.4516990

[16] Hexner, G., and Shima, T., "Stochastic Optimal Control Guidance Law with Bounded Acceleration," *IEEE Transactions on Aerospace and Electronic Systems*, Vol. 43, No. 1, 2007, pp. 71–78. doi:10.1109/TAES.2007.357155

[17] Shinar, J., and Shima, T., "Non-Orthodox Guidance Law Development Approach for Intercepting Maneuvering Targets," *Journal of Guidance, Control, and Dynamics*, Vol. 25, No. 4, 2002, pp. 658–666. doi:10.2514/2.4960

[18] Shaviv, I. G., and Oshman, Y., "Estimation-Guided Guidance," AIAA Paper 2006-6217, 2006.

[19] Shinar, J., Oshman, Y., Turetsky, V., and Evers, J., "On the Need for Integrated Estimation/Guidance Design for Hit-to-Kill Accuracy," *Proceedings of the 2003 American Control Conference*, Vol. 1, June 2003, pp. 402–407. doi:10.1109/ACC.2003.1238982

[20] Rusnak, I., "Multiple Model-Based Terminal Guidance Law," *Journal of Guidance, Control, and Dynamics*, Vol. 23, No. 4, 2000, pp. 742–746. doi:10.2514/2.4593

[21] Gelb, A., and Vander Velde, W. E., *Multiple-Input Describing Functions and Nonlinear System Design*, McGraw–Hill, New York, 1968, pp. 365–385.

[22] Gokcek, C., Kabamba, P. T., and Meerkov, S. M., "An LQR/LQG Theory for Systems with Saturating Actuators," *IEEE Transactions on Automatic Control*, Vol. 46, No. 10, 2001, pp. 1529–1542. doi:10.1109/9.956049

[23] Jacobson, D. H., and Mayne, D. Q., *Differential Dynamic Programming*, Elsevier, New York, 1970.